MICROFABRICATED OPTICAL SENSOR PROBE FOR THE DETECTION OF ESOPHAGEAL CANCER

A Thesis

by

KARTHIK REDDY CHINNA BALAREDDY

Submitted to the Office of Graduate Studies of
Texas A&M University
in partial fulfillment of the requirements for the degree of

MASTER OF SCIENCE

May 2009

Major Subject: Electrical Engineering

MICROFABRICATED OPTICAL SENSOR PROBE FOR THE DETECTION OF ESOPHAGEAL CANCER

A Thesis

by

KARTHIK REDDY CHINNA BALAREDDY

Submitted to the Office of Graduate Studies of
Texas A&M University
in partial fulfillment of the requirements for the degree of

MASTER OF SCIENCE

Approved by:

Chair of Committee,	Jun Zou
Committee Members,	Mosong Cheng
	Steven Wright
	Wonmuk Hwang
Head of Department,	Costas N. Georghiades

May 2009

Major Subject: Electrical Engineering

ABSTRACT

Microfabricated Optical Sensor Probe for the Detection of Esophageal Cancer.

(May 2009)

Karthik Reddy Chinna Balareddy, B.S., Texas A&M University

Chair of Advisory Committee: Dr. Jun Zou

Cancer is a class of diseases in which a group of cells grow uncontrollably, destroy surrounding tissue and eventually spread to other parts of the body, often leading to death. According to the American Cancer Society cancer causes accounts for 13% of all deaths. Much of the time cancer can be treated if diagnosed early. Considerable study is currently being undertaken to investigate tissue properties and their use in detecting cancer at an early stage through non invasive and non surgical methods. Oblique Incidence Diffuse Reflectance Spectrometry (OIDRS) is one such method.

This thesis reports the design, fabrication and testing of a new miniaturized optical sensor probe with "side viewing" capability for oblique incidence diffuse reflectance spectrometry. The sensor probe consists of a lithographically patterned polymer waveguides chip and three micromachined positioning substrates and source/collection fibers to achieve 45^{o} light incidence and collection of spatially resolved diffuse reflectance.

The probe was tested at the Mayo Clinic in Rochester Minnesota. The test results show that the probe is capable of collecting data which can be analyzed to select image

features to differentiate the cancerous tissue from non cancerous tissue. Using these probes, diffuse reflectance of human esophageal surface has been successfully measured for differentiation of cancerous tissues from normal ones.

DEDICATION

To my parents, grandparents and brother

ACKNOWLEDGEMENTS

I would like to thank my committee chair, Dr. Zou, my committee members, Dr. Cheng, Dr. Wright, Dr. Hwang, and my colleague Alejandro Garcia-Uribe for their guidance and support throughout the course of this research.

Thanks also go to my friends and colleagues, the department faculty and staff, all my professors and the Spirit of Aggieland for making my time at Texas A&M University a unique and extremely gratifying experience.

Finally, thanks to family, in particular my father Venkataramana Reddy, my mother Sandhya Reddy and my brother Gautham Reddy, for their support and encouragement.

NOMENCLATURE

OIDRS	Oblique Incidence Diffuse Reflectance Spectrometry
OIR	Oblique Incidence Reflectometry
GE	Gastroesphageal
GERD	Gastroesophageal Reflux Disease
SNR	Signal to Noise Ratio

TABLE OF CONTENTS

CHAPTER Page

LIST OF FIGURES

FIGURE Page

LIST OF TABLES

CHAPTER I

INTRODUCTION

Cancer

Cancer is a class of diseases in which cells multiply uncontrollably, kill surrounding tissue and in some cases spread to other parts of the body through lymph or blood. Cancer is essentially an abnormality in the genetic material of the cells. These genetic abnormalities can be influenced or may be caused by factors that include smoke inhalation, radiation, infectious agents, chemicals, errors in genetic replication or inherited defects.

According to the American Cancer Society about 7.6 million people, across the world, die from cancer every year [1]. This reflects about 13% of all deaths. If left untreated they often prove fatal, but with early diagnosis and proper treatment it can be treated effectively, in most cases.

Esophageal Cancer

The esophagus is muscular tube that connects the oral cavity to the ventriculus. Its primary function is to transport food, water and other liquids to the ventriculus. On average the esophagus is 12-13 inches long and is usually greater than three quarters of an inch across. It is divided into cervical, thoracic, and abdominal sections.

The wall of the esophagus consists of several layers. Esophageal cancer usually starts from its inner layer and grows outward. The innermost layer of the esophagus is

---

This dissertation follows the style of *Lab on a Chip*.

called the mucosa. The mucosa has 2 parts, the epithelium and the lamina propria. The lining of the esophagus is called the epithelium and is made up of flat, thin cells called squamous cells. The lamina propria is a thin layer of connective tissue right under the epithelium.

The next layer is the submucosa. In some regions the esophagus has mucus-secreting glands in this layer. Under the submucosa is a thick band of muscle called the muscularis propria. This is the layer which is responsible for forcing food down the esophagus from the mouth to the stomach through coordinated and rhythmic contraction of muscleslayer. The outermost layer of the esophagus, which is called the adventitia, is formed by connective tissue.

In the upper region of the esophagus there is a special area of muscle that relaxes to open the esophagus when it senses food or liquid coming toward it. This muscle is called the upper esophageal sphincter. The lower part of the esophagus that connects to the stomach is called the gastroesophageal junction, or GE junction. As with the upper region there is a special area of muscle near the GE junction called the lower esophageal sphincter. The purpose of the lower esophageal sphincter is to control the movement of food from the esophagus into the stomach while keeping the stomach's acid and digestive enzymes out of the esophagus. The structure of the esophagus is illustrated in figure 1.

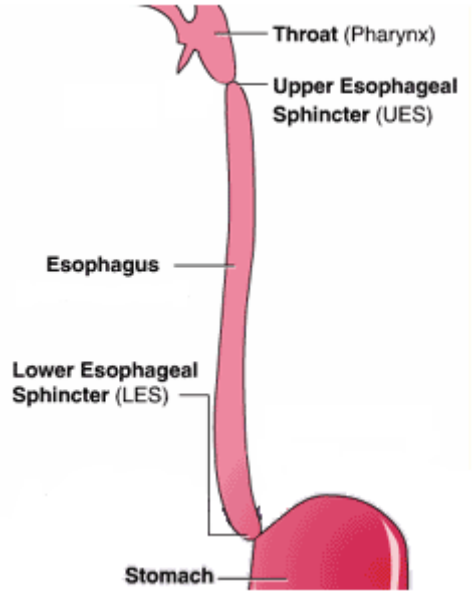

Fig. 1. Diagram of the structure of the esophagus

The stomach contains powerful acid and enzymes that are necessary for the digestion of food. The epithelium (lining of the stomach) is made of glandular cells that release the required acid, enzymes, and mucus. These cells have special features that protect them from the acid and digestive enzymes.

Sometimes, acid can escape from the stomach into the esophagus. This phenomenon is medically termed as reflux or gastroesophageal reflux disease (GERD). The normal symptoms of reflux include heartburn or a burning sensation that radiates from the middle of the chest. However, in some cases, reflux can be symptom less. If the stomach acid remains in the lower esophagus for an extended period of time, the acid can cause damage to the lining of the esophagus, leading to abnormal glandular cells replacing the squamous cells that usually line the esophagus. These glandular cells are similar in appearance to the cells that line the stomach and are more resistant to stomach

acid than the cells they have replaced. When these glandular cells are present in a person's esophagus, the condition is called Barrett's esophagus. People with Barrett's esophagus have a much greater chance of developing cancer of the esophagus (estimated at 30-100 x normal). Even with the elevated risk, most people with Barrett's esophagus still do not go on to develop esophageal cancer.

There are 2 main types of esophageal cancer, squamous cell carcinoma and adenocarcinoma. Since the entire esophagus is lined with squamous cells, squamous cell carcinoma can occur anywhere along the length of the esophagus. Until recently, in the United States, Squamous cell carcinoma was far more common of than adenocarcinoma, and was responsible for almost 90% of all esophageal cancers. But recent statistics show, squamous cell cancers make up less than 50% of esophageal cancers.

Adenocarcinoma forms in glandular tissue, which normally does not exist as the cover of the esophagus. Before adenocarcinoma can develop in the esophagus, glandular cells must replace an area of squamous cells, as in the case of Barrett's esophagus, shown in figure 2. As Barrett's esophagus mainly occurs in the lower regions of the esophagus, this is also the region where adenocarcinoma is found.

According to the American Cancer Society, there were around 16,470 new cases of esophageal cancers with about 14,280 deaths in 2008 [1]. Some countries such as Iran, northern China, India, and southern Africa have occurrence rates 10-100 times higher than that of the United States [1]. Because esophageal cancer is usually diagnosed at a late stage, most people with esophageal cancer eventually die of this disease. Therefore,

there is an urgent need for early diagnosis techniques, which are accurate, non-invasive and low-cost.

Fig. 2. Barrett's esophagus in lower esophagus [2]

Clinical Diagnosis of Esophageal Cancer

The tradition and most important test for diagnosing esophageal cancer is upper endoscopy. This procedure involves the use of a gastroscope, a endoscope specially designed for gastroenterology applications. Typically a gastroscope consists of a flexible tube with a light guide for illumination, an objective lens and a camera for video capture, an air/water nozzle for cleaning the lens, and an instrument channel to accept a series of accessories for biopsy and other treatment purposes. Once inserted into the GI tract, the flexible tube can be rotated along its axis and the distal end can have a 2-way angulation for efficient examination of esophagus and other portions of the GI tract. A tissue sample can be taken through the endoscope for laboratory testing to determine whether it is

cancerous and which type of cancer.

People with strong risk factors for esophageal cancer should have periodic endoscopic biopsy surveillance. Patients with Barrett's esophagus should have four quadrant biopsies at every one or two centimeter intervals along the entire length of the Barrett's lining. The reason for taking four quadrant biopsies is that by sampling all four walls of the esophagus odds of missing a small area of abnormal cells that can only be seen by examination under a microscope and not through the endoscope is decreased. According to the current recommendations for patients who have a stable negative diagnosis for dysplasia, is that they come back every 3 years for follow-up endoscopic biopsy surveillance and for patients who have a stable diagnosis of low-grade dysplasia, it is recommended that they return yearly for endoscopic biopsy surveillance until they have a set of biopsies in which no dysplasia is detected.

The possibility that a patient who has a diagnosis of high-grade dysplasia already has a cancer that will not be detected until it is advanced and incurable with surgery, is a major concern. Maintaining a facility to conduct intensive and frequent is extremely expensive and not suitable for most gastroentologists. The biopsy may also cause bleeding and discomfort to the patients. Hence many patients who develop esophageal adenocarcinoma are not in a cancer surveillance program. As a result, endoscopic biopsy surveillance has not favorably impacted the mortality rate of esophageal cancer.

Esophageal cancers are very difficult to diagnose at the early and curable stage. Endoscopic biopsy surveillance is currently the only widespread procedure to monitor the development of esophageal cancers for people with strong risk factors. However, its

effectiveness is hampered by the complexity and cost of the procedure, as well as possible complications and discomfort caused by the biopsy. To overcome the shortcomings of endoscopic methods being used at present**,** it is highly necessary to investigate new techniques to greatly reduce the complexity and cost of the surveillance procedures. The new techniques should be completely non-invasive, fast and simple to use.

Non-invasive Optical Methods of Diagnosis

Much research is currently being conducted using fluorescence spectroscopy to detect the disease states of tissue based on the fact that fluorescence, being a manifestation of the biochemical environment of the cell, should be a specific indicator of cellular alterations due to disease [3, 4]. By contrast, because of the highly turbid nature of biological tissues, the bulk optical transport properties of tissue may be only slightly changed by a localized pathological process, thus reducing the sensitivity of scattering and absorption as specific measures of disease. Nevertheless, a number of recent reports have found that light scattering or reflectance measurements, either alone or in conjunction with fluorescence spectroscopy, are capable of distinguishing pathologic changes in tissue such as the skin [3, 4, 5], cervical tissue [6, 7], GI tract [8, 9], and breast [10, 11].

When we view the surface of biological tissues with naked eye, we cannot separate the absorption and scattering effects of the tissue on light. Normal-incidence reflectometry can separate the two effects but only with absolute measurements of the

diffuse reflectance, which are difficult to obtain reliably in a clinical setting. Unlike normal-incidence reflectometry, OIR breaks the symmetry in the diffuse reflectance pattern and by using OIR it is possible to quantify both the absorption and scattering optical properties based on relative measurements alone, and is therefore very robust and suitable for clinical applications. By measuring the diffuse reflectance of a biological tissue with OIR, important optical properties, such as the absorption and reduced scattering coefficients, can be extracted [12]. Previous studies, found that these optical properties are closely related to some of the key diagnostic physiological parameters of the tissue which significantly vary with its exact disease state, including (1) the oxygen saturation of hemoglobin, (2) the concentration of total hemoglobin, and (3) the cell-nuclear size [13, 14, 15]. Therefore, OIR could become a very accurate non-invasive imaging tool to detect and differentiate different lesions on the surface of tissues and organs.

CHAPTER II

OBLIQUE INCIDENCE DIFFUSE REFLECTANCE SPECTOMETRY

Absorption and Scattering of Light by Tissue

As shown in Fig. 3, when light is incident on the surface of an heterogeneous media (e.g. human skin), part of the incident light will be directly reflected (specular reflectance) and the remaining light will transmit into and interact with the media. After undergoing multiples times of scattering and absorption, part of the transmitted light will be turned back and escape from the surface the media. This light which escapes forms the diffuse reflectance.

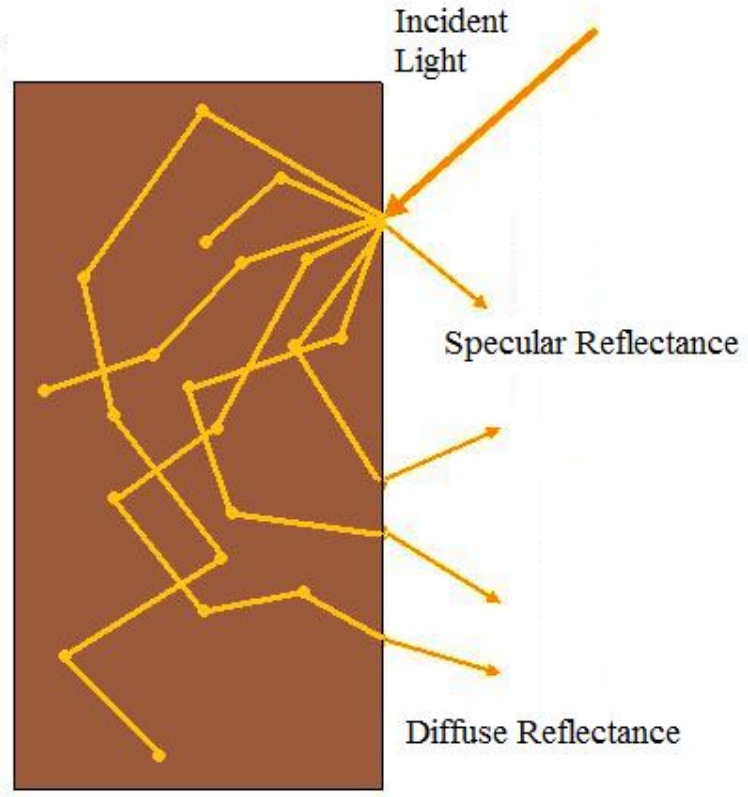

Fig. 3. Interaction of light with a heterogeneous medium

According to the diffusion theory, the spatially resolved steady-state diffuse reflectance at certain wavelength ($R_d(x)$) for oblique incidence can be calculated using a modified two-source approximation with one positive source located below the sample surface and one negative located above the sample surface (Fig. 4) [12, 16], which can be determined by

$$R_d(x) = \frac{1}{4\pi}\left[\frac{\Delta z(1+\mu_{eff}\rho_1)\exp(-\mu_{eff}\rho_1)}{\rho_1^3} + \frac{(\Delta z + 2z_b)(1+\mu_{eff}\rho_2)\exp(-\mu_{eff}\rho_2)}{\rho_2^3}\right] \quad (1)$$

where μ_{eff} is the effective attenuation coefficient, ρ_1 and ρ_2 are the distances between the two isotropic point sources (one positive source located below the media surface and one negative source above the media surface) and the observation point the surface of the media, Δz is the distance between the virtual boundary and the media depth, and z_b is the distance between the virtual boundary and the surface of the media. The absorption coefficient (μ_a) and reduced scattering coefficient (μ_s') can be determined as [17].

$$\mu_a = \frac{\mu_{eff}^2 \Delta x}{3\sin(\alpha_t)} \quad (2)$$

$$\mu_s' = \frac{\sin(\alpha_t)}{\Delta x} - 0.35\mu_a \quad (3)$$

where Δx is the shift of the point sources in the x direction for the modified dipole source diffusion theory model, α_t is the angle of light transmission into the medium. By capturing the spatial distribution of diffuse reflectance ($R_d(x)$) the optical properties μ_a and μ_s' can thus be calculated by solving the inverse problem [18]. The diffusion-theory-based model is only valid if the reduced scattering coefficient is much larger than the

absorption coefficient [19] as is the case in biological tissue. Also, the source and detector must be separated such that the light consists of diffuse reflectance when it reaches the detector.

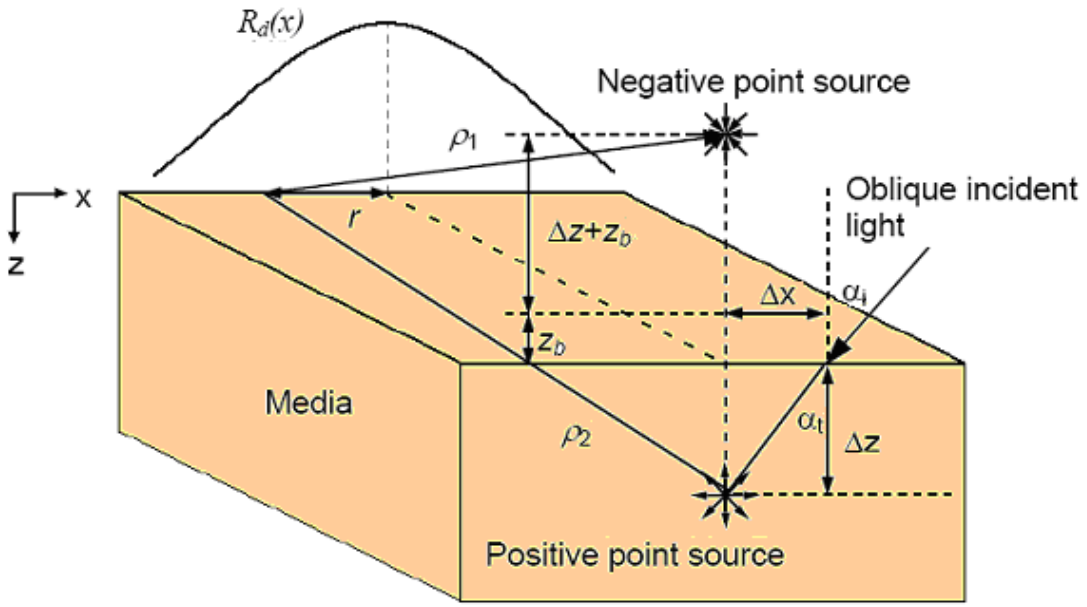

Fig. 4. Schematic of the modified two-source approximation of oblique incidence based on the diffusion theory

OIDRS Experimental System Setup

To conduct OIDRS measurement, a complete experimental setup, to interface with a sensor probe, has been built to achieve automated optical incidence control, data collection and analysis (Fig. 5). A standard sensor probe consists of 1 to 3 source fibers and several, usually in the range of 8-20, collection fibers. The system consists of a halogen lamp which acts as a white light source for multiple-wavelength measurement, multiplexer, imaging spectrograph, personal computer, and CCD camera. The 16-bit Andor Technology 412DV CCD camera has a 512 x 512-pixel CCD chip with

dimensions of 12.6 x 12.6 mm^2. With this chip size and a 150-lines/mm grating it is capable of imaging wavelengths in the range of 310 nm onto the CCD matrix. Before an OIDRS measurement is conducted, the source fiber of the sensor probe is connected to the output of the light source via an SMA connector. The proximal end of each of the interconnection fibers is also fitted with SMA 905 connectors and then connected to the input of the spectrograph through a custom-made interface. The optical multiplexer allows light to be delivered, to the area of interest, through only one source fiber at a time. After the sensor probe is placed in contact with the sample surface, white light is delivered through the source fiber and the diffuse reflectance is then collected by the waveguides or fibers and coupled to the imaging spectrograph which generates an optical spectrum for each collection channel. The CCD camera collects the spectral-images from the wavelength range of 455 to 765 nm. The spectral images represent the steady-state diffuse reflectance spectra from each collection channel. These spectra are stored in the computer for further analysis. This entire OIDRS system is capable of capturing one frame of spectral image in a fraction of a second.

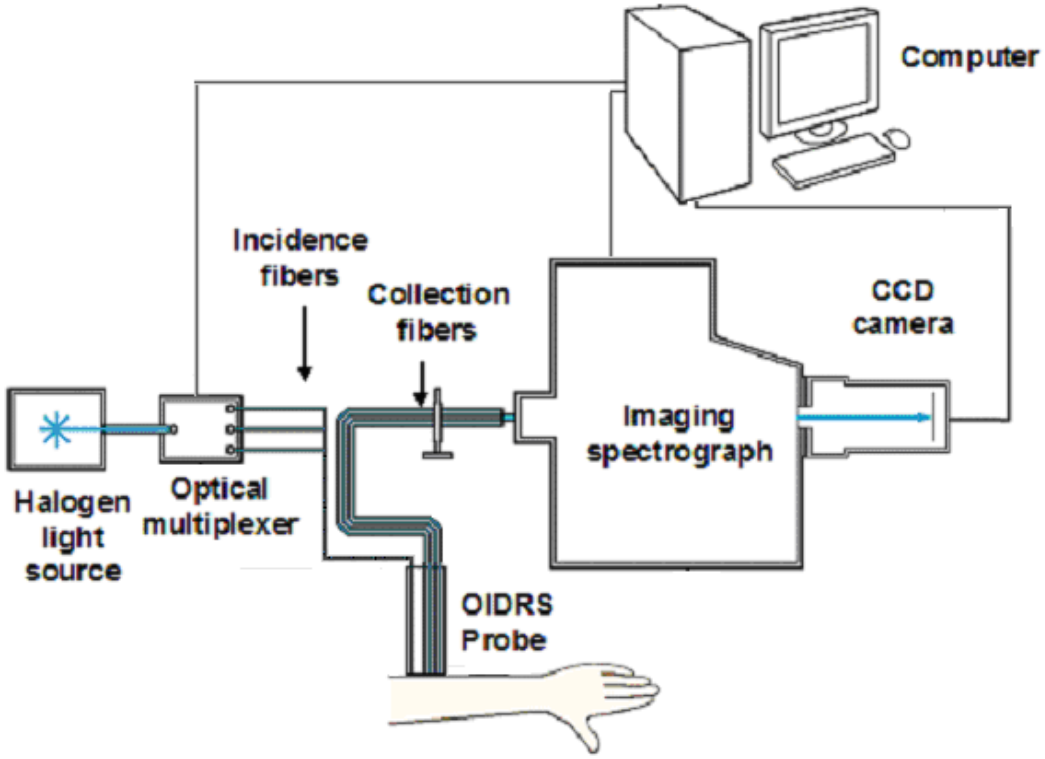

Fig. 5. OIDRS system with skin cancer probe attachment

In-Vivo Testing of OIDRS System on Skin Cancer

The testing on human skin was performed at the University of Texas M.D. Anderson Cancer Center in Houston. The collected OIDRS images were divided into two abnormality groups. The pigmented group consisted the following cancerous, dysplastic and benign subgroups (1) melanoma in situ and invasive melanoma (M), (2) mild dysplastic nevi (DN1), moderate dysplastic nevi (DN2), severe dysplastic nevi (DN3) and (3) common Nevi,(CN), actinic keratosis (AK,) seborrheic keratosis (SK). The non-pigmented group consisted of the following cancerous and benign subgroups (1)

basal cell carcinomas (BCC) and squamous cell carcinomas (SCC) and (2) actinic keratosis (AK,) seborrheic keratosis (SK).

Data was collected from 167 pigmented and 78 non-pigmented skin lesions. Of the pigmented group 16 lesions were diagnosed by standard techniques as melanoma and for the non pigmented group, 35 lesions were diagnosed as carcinoma. The number of lesions of each type for pigmented and non-pigmented samples are shown in Tables I and II respectively.

Table I. Pigmented skin lesions.

Type of lesion	#
Melanoma (M)	16
Severe dysplastic nevi (DN3)	8
Moderate dysplastic nevi (DN2)	61
Mild dysplastic nevi (DN1)	30
Common nevi (CN)	31
Actinic keratosis (AK)	5
Seborrheic keratosis (SK)	16
Total	167

Table II. Non-pigmented skin lesions.

Type of lesion	#
Basal cell carcinoma (BCC)	35
Squamous cell carcinoma (SCC)	21
Actinic keratosis (AK)	17
Seborrheic keratosis (SK)	5
Total	78

For the pigmented lesion group, one classifier separates the malignant lesion subgroup from the benign lesion subgroup, and precancerous subgroup.

For the non-pigmented group, a single classifier was used to separate basal cell carcinomas (BCC) and squamous cell carcinomas (SCC) from actinic keratosis (AK,) seborrheic keratosis (SK). The classifier generated an overall classification rate of 95% with 97% sensitivity and 91% specificity as shown in Tables III and IV.

Table III. Classification of pigmented lesions

	DN1, DN2, DN3	CN, AK, SK	Hit Rate %
DN1, DN2, DN3	95	4	96
CN, AK, SK	10	42	81

Table IV Classification of non-pigmented lesions

	BCC, SCC	AK, SK	Hit Rate %
BCC, SCC	54	2	97
AK, SK	2	20	91

CHAPTER III

ROLE OF MICROFABRICATION IN OIDRS

Design of Skin Cancer Probe

To conduct OIDRS measurement on human skins, a hand-held fiber optical sensor probe has been developed to facilitate convenient and robust data collection in a clinical environment. The sensor probe consists of three source fibers and two linear arrays of collection fibers for capturing the spatial distribution of diffuse reflectance. The effective probe testing area is limited to 2×2 mm^2 to ensure that the measured area does not include the surrounding normal skin even for the smallest skin lesions which are usually around 3×3 mm^2. Among the three source fibers, two are used for oblique incidence, each one capable of delivering light to the skin surface at an angle of incidence of 45^o. Since the OIDRS measurement is usually performed in a dark environment to reduce the effect of the background light, the middle fiber which is aligned with the normal is used to illuminate area of interest on the skin to ensure the accurate placement of the sensor probe. Although only one oblique incidence fiber and one linear array of collection fibers are necessary for an OIDRS measurement, two oblique incidence fibers and two arrays of collection fibers are used for multiple data collections from the same location on the skin to ensure a reliable and robust measurement.

To provide sufficient light to the area of interest, and ensure a high signal to noise ratio of the measurement, the source fibers used have a diameter of 200 μm.

Ensuring a high signal to noise rations is especially important for dark colored skins. For the collection fibers, each of the two linear arrays consists of 10 fibers with a diameter of 100 μm and a center-to-center pitch of 200 μm. Based on previous simulations, at least 8 data points are needed for a span of 2 mm to achieve a good spatial resolution for the estimation of the optical absorption and scattering properties with good accuracy. The 100 μm diameter of the collection fibers is expected to provide satisfactory SNR for the measurement of diffuse reflectance. The use of smaller collection fibers will result in lower SNR and the use of bigger collection fibers would unnecessarily increase the size of the probe or lower the spatial resolution of data sampling. Due to the 500 μm thickness of each silicon substrate, the two collection fiber arrays are separated from the incidence fibers by 1 mm, as shown in figure 6. This is necessary because the estimation of the absorption and scattering coefficients from the measured diffuse reflectance is based on the Diffusion Theory, which is accurate only when the distance between the detector and the source is greater than one mean free path $L_t' = 1/(\mu_a+\mu_s')$ (typically about 0.1 cm for biological tissues [20]. Although larger separation could be used, it will unnecessarily increase the overall size of the sensor probe. [21]

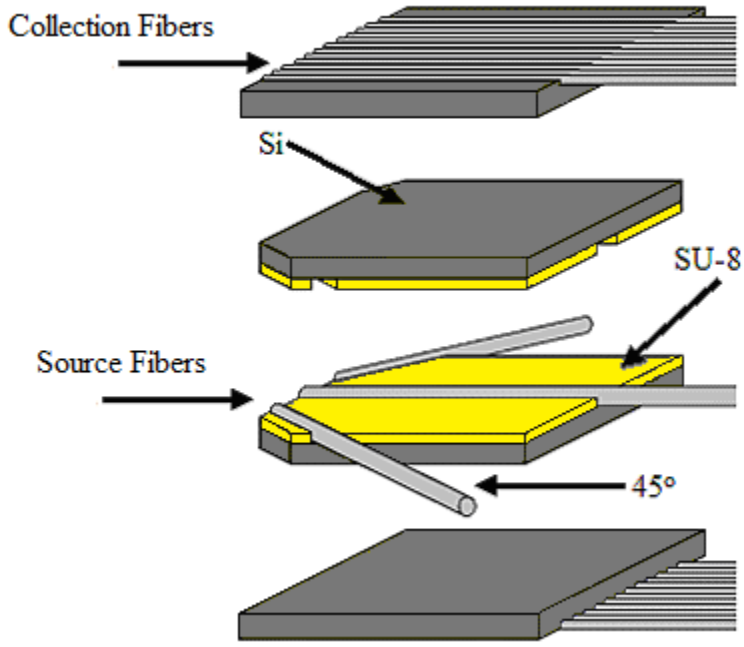

Fig. 6. Skin cancer probe design

To ensure the accuracy of the OIDRS measurements, the source fibers and collection fibers need to be precisely aligned with respect to each other and fixed in their own positions. This can be achieved with a compact mechanical positioning device. However, due to the small size and dense arrangement of the fibers, it is very difficult and costly to fabricate the mechanical positioning device using conventional machining methods. To address this issue, a straightforward micromachining processes was developed and used to successfully fabricate the positioning devices in an efficient and low-cost manner.

Fabrication of Skin Cancer Probe

To achieve accurate alignment of the collection fibers, two micromachined positioning devices ware fabricated. Each positioning device consists of a silicon substrate with a linear array of V-grooves created with silicon bulk etching (Fig. 4a). When an optical fiber (with cylindrical cross-section) is placed in a V-groove, the center axis of the optical fiber can "automatically" align with the symmetric plane of the V-groove. Thus, the accurate positioning of each collection fiber in the array can be readily achieved to ensure reliable and uniform performance of the sensor probe.

For aligning the source fibers, two other micromachined positioning devices are fabricated. Since the need of guiding structures for the oblique incidence fibers (45^{o}) precludes the fabrication of V-grooves with silicon bulk etching, SU-8 resist (MicroChem, MA) was used for the fabrication of the guiding structures on a silicon substrate. SU-8 is preferable for this process as it can be directly used to form structures over 100 μm in thickness, which results in a very simple and low-cost fabrication process.

After the fabrication of the micro positioning devices is completed, the entire OIDRS sensor probe is assembled. First, both the source and collection fibers are fixed into their own guiding structures. Since the thickness of the SU-8 guiding structure is 100 μm, two positioning devices can be placed face-to-face to accommodate the source fibers (with a diameter of 200 μm). For the collection fibers, one positioning device and one cover substrate were used to hold them in place. After all the fibers are assembled, the positioning devices were stacked and glued together with epoxy. Since the thickness

of the silicon wafer used for the fabrication of the positioning devices is around 500 μm, the required 1 mm spacing between the source and collection fibers is readily obtained. To improve the efficiency of incidence and collection of the fibers, the head of the assembled probe is polished with fine sand papers. During the polishing, care has to be taken to avoid any possible damage to the fibers. Finally, the assembled probe was placed in an aluminum probe holder to facilitate OIDRS testing. [21]

CHAPTER IV

SIDE VIEWING ESOPHAGEAL CANCER PROBE

Esophageal Cancer Probe Design

The skin probe assumes a front viewing configuration, in which the sensor head is in line with the direction of the source/collection fiber bundles. All the collection fibers remain straight and thus can be arranged in a dense manner with suitable spacing for capturing the spatial distribution of the diffuse reflectance. To accommodate the 45^{o} bending of the two source fiber for oblique incidence, an outer dimension of the probe (15×10 mm^2) is used to prevent sharp bending of the source fibers. For in-vivo skin testing, the "front viewing" configuration and the relatively large size of the probe are desirable for hand-held applications. However, for inner-body applications (e.g. esophagus), this configuration and dimension of sensor probe becomes an issue. First, to conduct effective and efficient in-vivo measurement inside the human body, the OIDRS probe has to be mounted onto a medical endoscope for manipulation and targeting. Current medical endoscopes can only accept tool attachments with diameters ranging from 2 to 5 mm. The current OIDRS probe is too bulky for this purpose. Second, while the "front viewing" configuration is ideal for skin applications, it will be difficult to use it to conduct in-vivo measurements in the tight inner-body cavities. A "side viewing" configuration will be preferable, in which the sensor head is oriented in a perpendicular position with respect to the axis of the fiber bundles (Fig. 7). However, this inevitably requires a sharp 90^{o} turn for all the collection fibers within a very tight space, which

would cause very high light loss and leakage (with cross-talk between adjacent collection channels) and also possible mechanical fracture of the collection fibers.

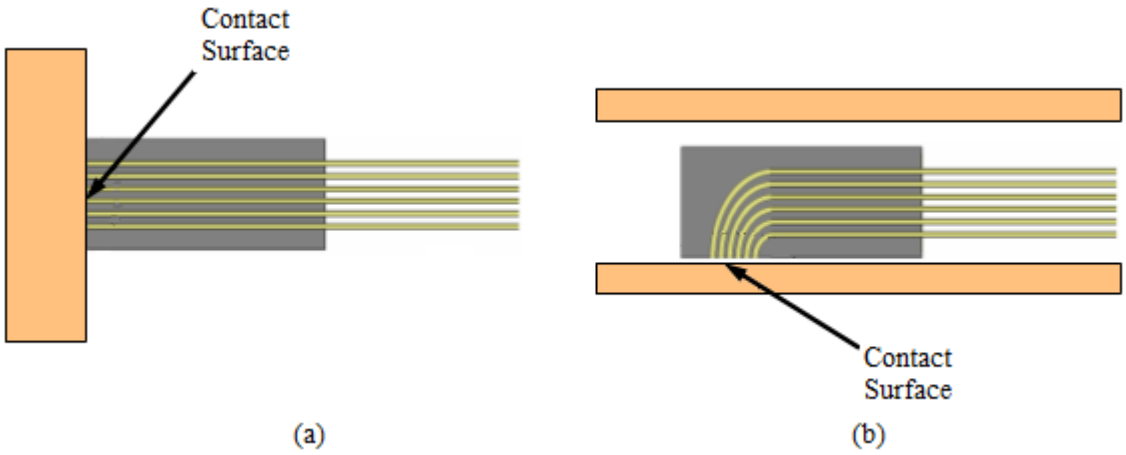

Fig. 7. a) Front viewing skin cancer probe b) Side viewing esophageal cancer probe

To address this issue, we have come up with a new 3-chip probe design with lithographically patterned polymer waveguides. This new probe design consists of three substrates. The first substrate serves as the positioning device to guide the source fiber for a 45^{o} oblique incidence. To reduce the probe size, only one source fiber is used for oblique incidence. Since the endoscope already has built-in light source for illumination, the normal incidence fiber which was used in the skin probe, to illuminate the area of interest, will not be necessary. To avoid the detrimental effects of direct sharp bending of the collection fiber array, a second substrate with microfabricated polymer waveguides is used for collecting the diffuse reflectance (Fig. 8). The four side walls of curved polymer waveguides are coated with highly reflective layers to prevent possible

light leakage and cross-talk of the waveguides. To interface the waveguides to OIDRS image capture and processing setup, a third substrate with bulk-etched V-groves is used to align the straight interconnection fiber bundles with exactly same pitch as that of the polymer waveguides (Fig. 9). [22]

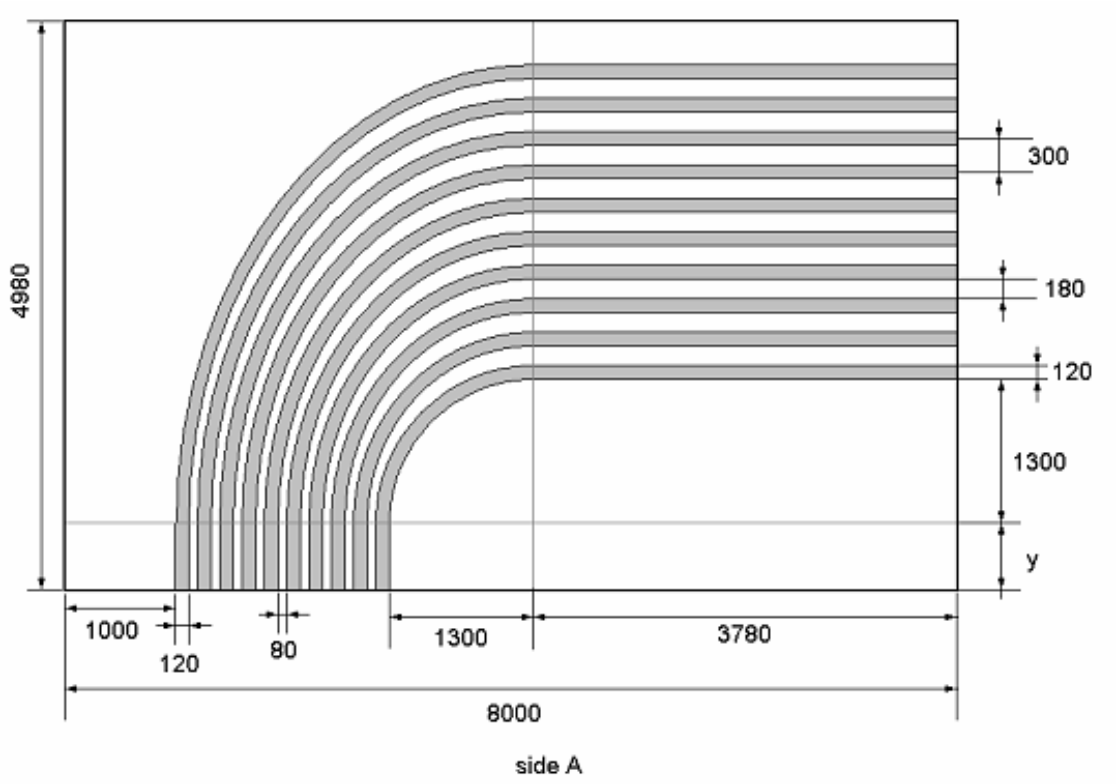

Fig. 8. Schematic design of SU-8 waveguide structures

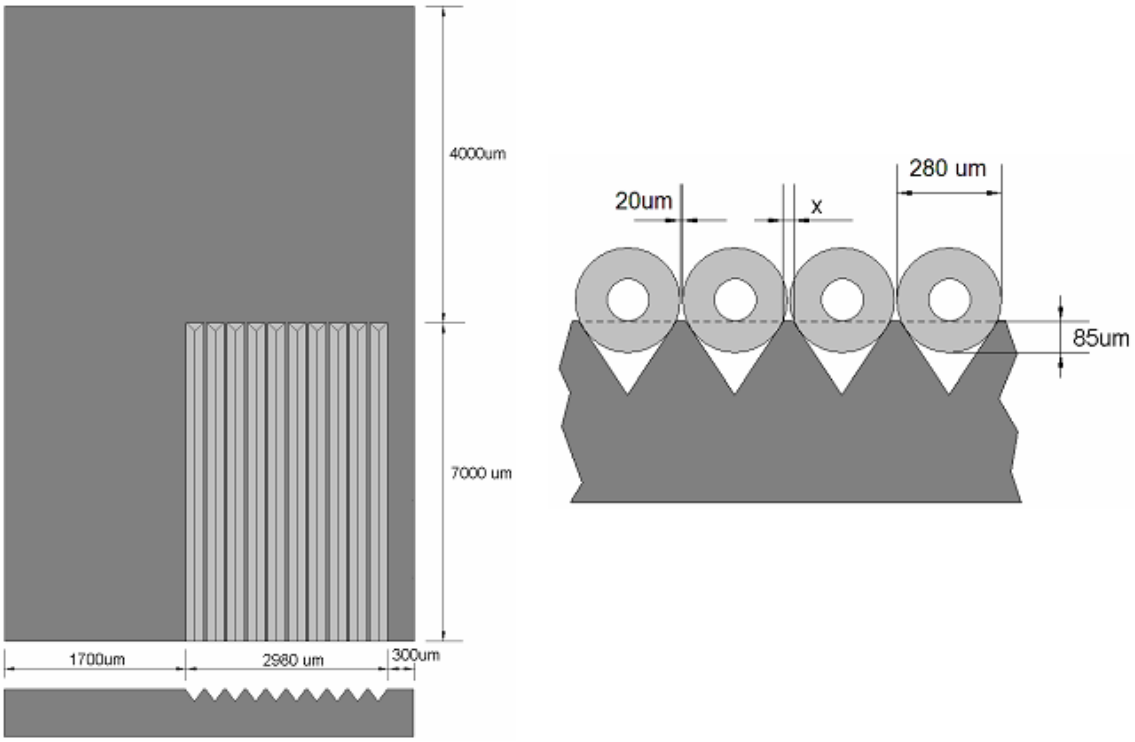

Fig. 9. Schematic design of bulk etched V-groove structures

Two masks were designed using L-Edit. A high resolution mask was made for SU-8 patterning and a transparency for the fabricating the bulk etched V-grooves (Figs. 10 and 11). Each mask contains many repetitions of the same patterns allowing for the fabrication of multiple probes at the same time, thereby reducing costs significantly.

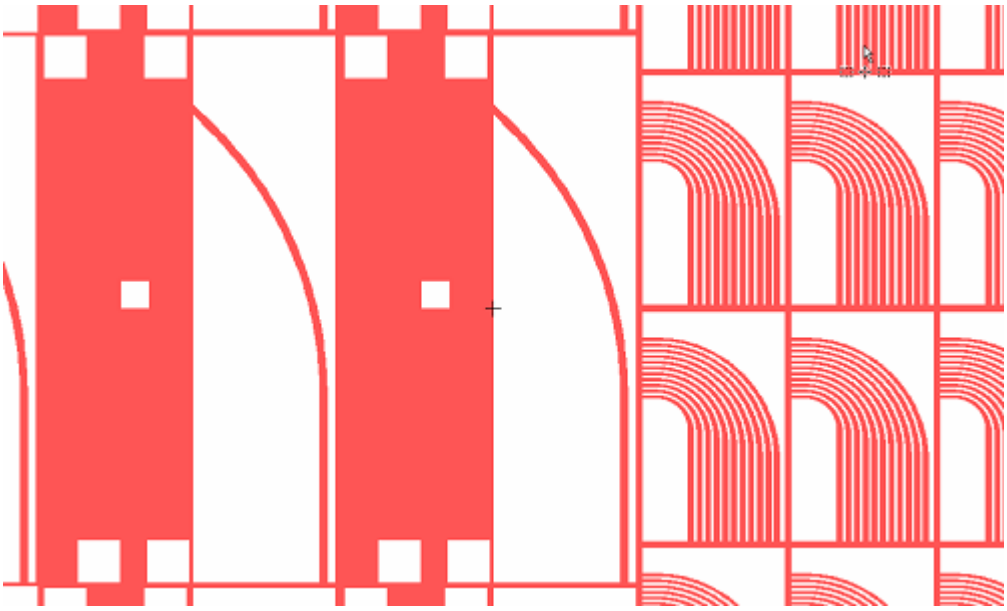

Fig. 10. Portion of mask design used for fabrication SU-8 structures

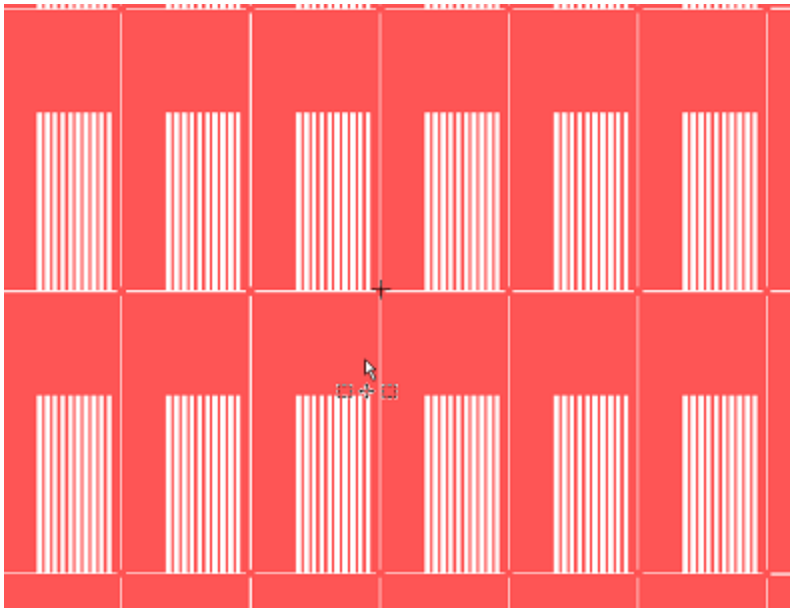

Fig. 11. Portion of mask design used for bulk etched structures

Esophageal Cancer Probe Fabrication

The OIDRS probe fabrication and assembly process consists of two steps: (1) fabrication of the three positioning substrates and (2) assembly of the source/collection fibers and device substrates. We chose SU-8 resist (MicroChem, MA) as structural materials for both the guiding structures of source fiber and also the curved waveguides for collecting the diffuse reflectance. First, SU-8 can be directly lithographically patterned to form thick and high-aspect-ratio microstructures (100 ~ 250 μm). Second, although it is not one of the most optically transparent polymer materials, SU-8 can still provide acceptable optical transmittance over the visible light spectrum for conducting OIDRS. Figure 12 shows the transmittance of visible light through a 100 micron thick layer of SU-8. The use of SU-8 microstructures eliminates the need for expensive microfabrication equipment and complex process steps, which results in a straightforward and low-cost fabrication process. This is important for future clinical application of OIDRS since the probe will be the only consumable part of the entire OIDRS system and it will be highly desirable to make it low-cost and thus disposable after a certain amount of use.

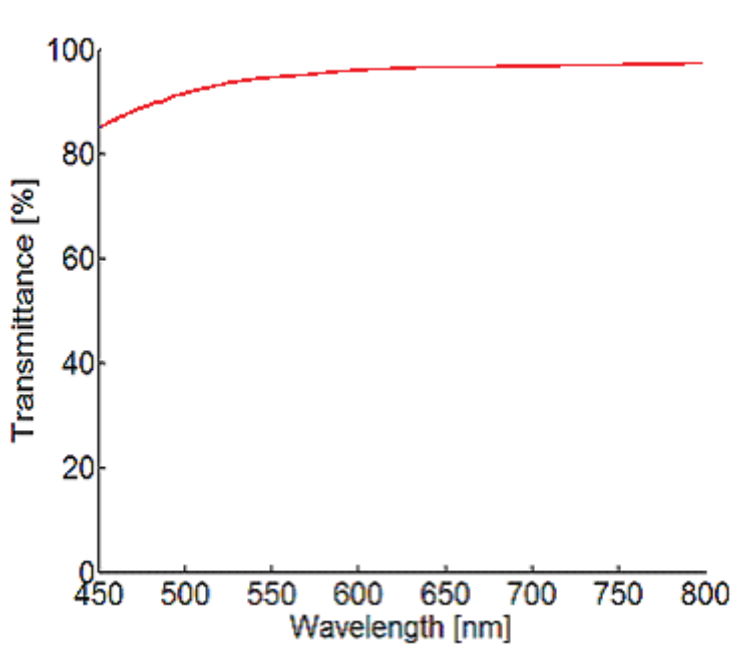

Fig. 12. Transmittance of SU-8 relative to wavelength

To align the source fiber (200 μm in diameter) to the 45^{o} oblique incidence angle, the first micro positioning substrate chip, with 100-μm-thick SU-8 guide structures was fabricated. SU-8 100 resist was spun on a pre-cleaned silicon wafer (500 μm thick) at calibrated spinning rate to reach a final thickness of about 100 μm. After SU-8 is deposited through spin-coating, a process recipe recommended by the manufacturer was followed to make the required guide structure with a 200-μm wide curved trench. The SU-8 first needs to be soft backed at 60 and 90 degree Celsius for 10 and 30 minutes respectively. The the SU-8 is photolithographically patterned at the near UV range and the patterned SU-8 is baked at 60 and 90 degrees for 1 and 10 minutes respectively. Finally SU-8 developer is used to remove the unexposed SU-8 giving us the required patterns. During the SU-8 processing, a slow temperature ramping was maintained to

minimize the internal stress build-up and also the resulting crack formation within the SU-8 film, which would significantly reduce the mechanical strength, stability and transmittance of the guiding structures.

Next, the above SU-8 process was repeated on another silicon wafer to make the 90^{o} curved collection waveguides (10 channels) with a cross-section area of 100×100 μm^2 each. To minimize light leakage and cross-talk between adjacent collection channels, the top, bottom and two side surfaces of the rectangular SU-8 waveguides were coated with thermally-evaporated aluminum (300 nm thick) in three consecutive steps. Before the SU-8 was deposited on the substrate, the bottom aluminum layer was deposited on the substrate using thermal evaporation method. After the SU-8 was fully processed and patterned, two more aluminum depositions were conducted with the substrate placed at an oblique $\pm 20^{o}$ with respect to the evaporation source to ensure a good coverage of the two side walls and the top surface (Fig. 13).

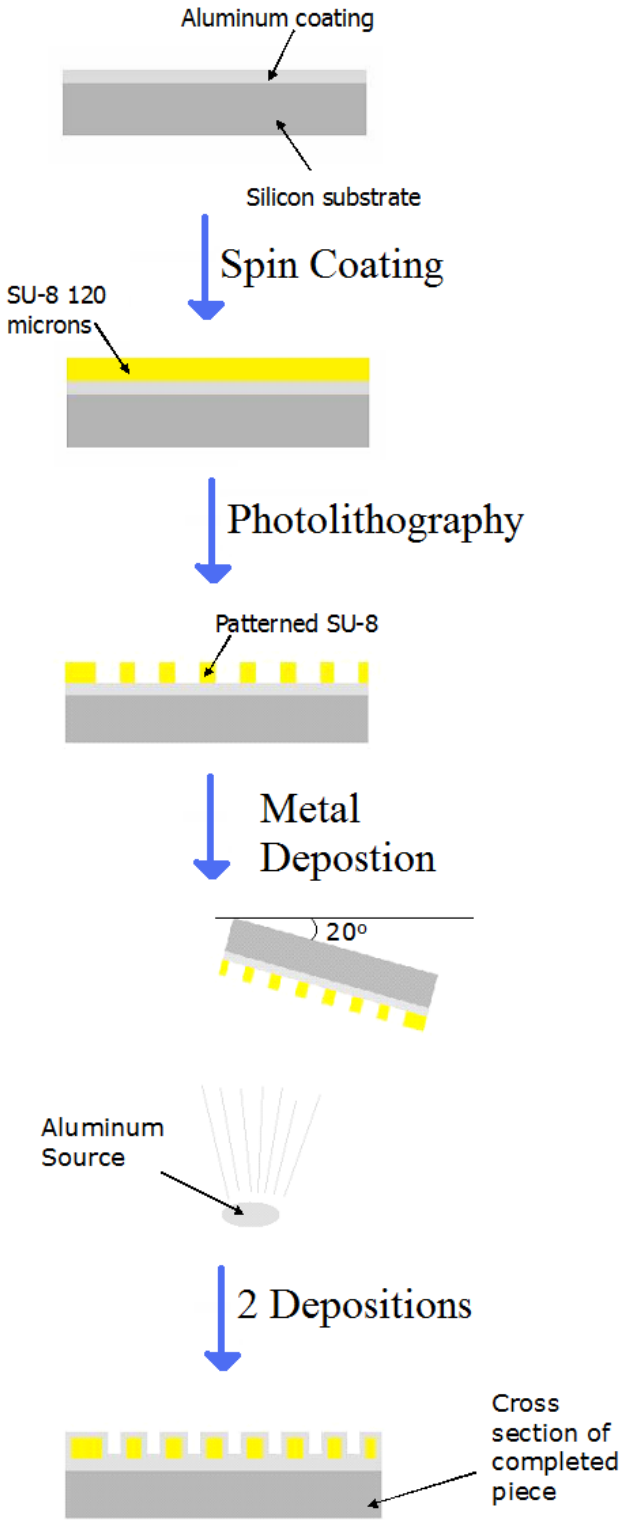

Fig. 13. Important processing steps for fabricating SU-8 structures

Finally, to accurately align the 100 micron diameter interconnection optical fibers, the third micro positioning substrate was fabricated. This chip consists of a silicon substrate with a linear array of V-grooves created with silicon bulk etching. When an optical fiber (with cylindrical cross-section) is placed in a V-groove, the center axis of the optical fiber can automatically align with the symmetric plane of the V-groove. Thus, the accurate positioning of the interconnection fibers can be readily achieved to ensure reliable and uniform performance of the sensor probe. [22]

To fabricate the positioning chip, silicon nitride was deposited on a {100} silicon wafer. Photolithography and patterning of AZ4620 photoresist was used to form a mask which enables the selective etching of the nitride layer using reactive ion etching. The selectively patterned nitride layer serves as a hard mask for silicon bulk etching. Silicon bulking etching was performed in potassium hydroxide solution to form the V-grooves (230 μm wide and 300 μm pitch) (Fig. 14).

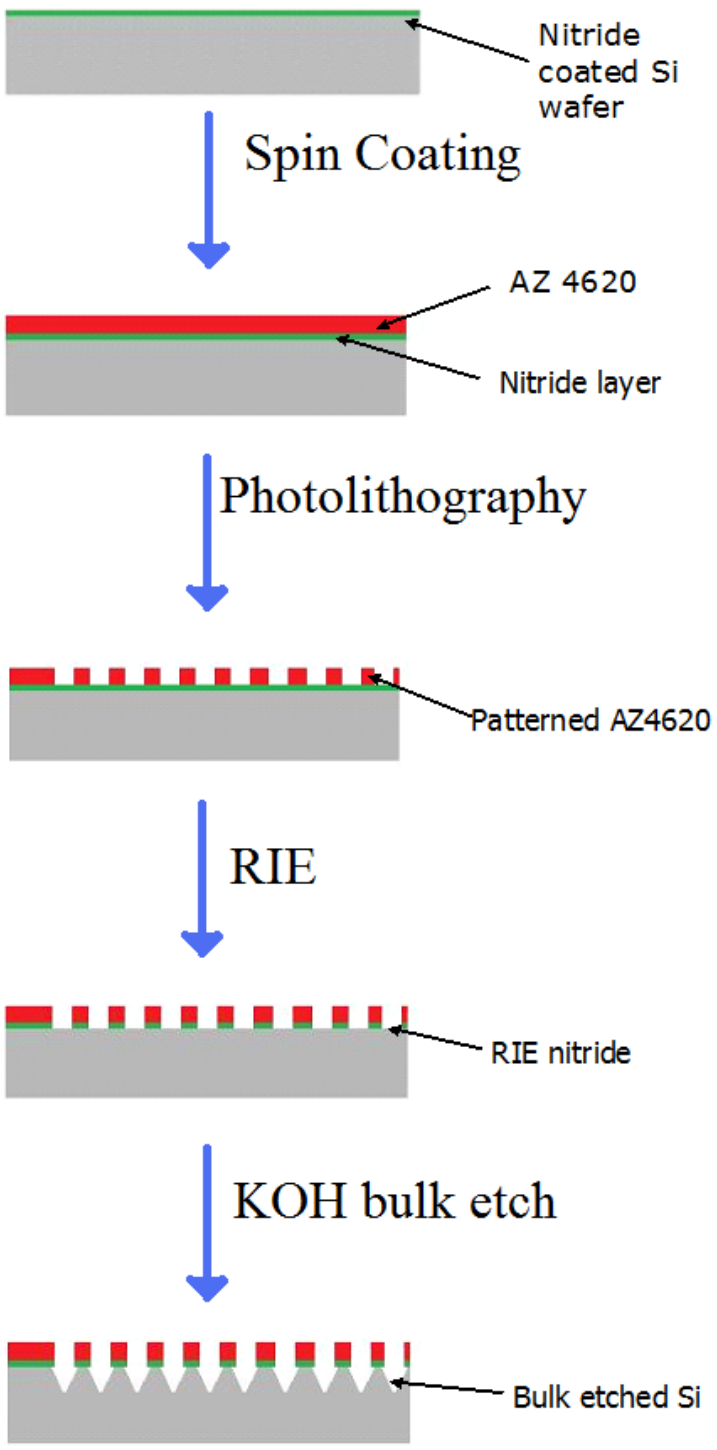

Fig. 14. Process steps for fabrication of bulk etched V-grooves

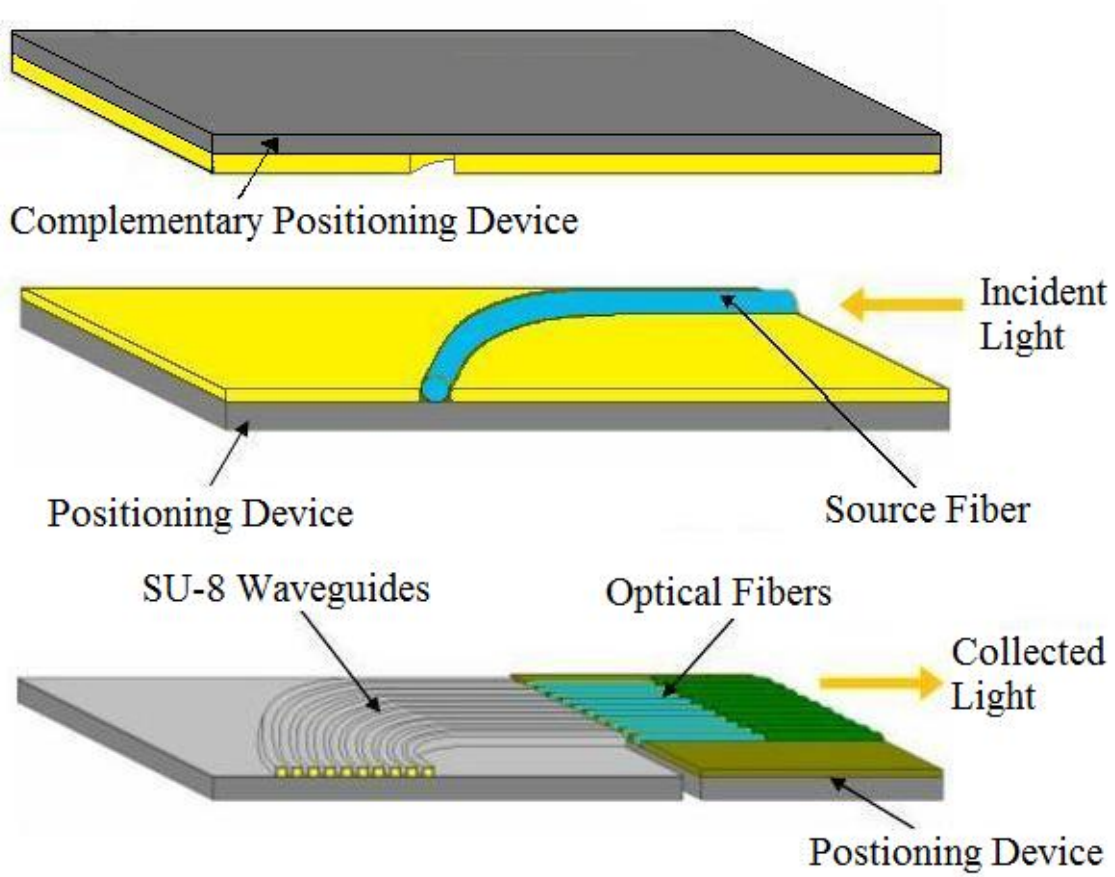

Fig. 15. Schematic of the "side-viewing" OIDRS probe assembly

After the fabrication, the entire probe could be assembled (Figs. 15 and 16). The source incidence fiber was carefully placed into the SU-8 alignment structure on the micro positioning substrate. A slow drying black epoxy was used to fix it in place. The interconnection fibers were similarly bonded into the V-groove structure using a slow drying black epoxy. To improve the efficiency of light incidence and collection of the optical fibers and SU-8 waveguides, the edge of the silicon chips with either input/output

end of the fibers or waveguides were carefully polished first with 2 μm and then 0.3 μm sand paper, while ensuring the structural integrity of the fiber or substrate were not compromised. After polishing, the SU-8 collection waveguides were aligned with the interconnection fibers. The position of the SU-8 waveguide chip was adjusted to couple the maximum amount of light coming out from the distal end of SU-8 waveguides. Once this was achieved, black epoxy was applied to bond the two chips together. The assembly of this probe is completed by stacking and gluing the source fiber substrate with the SU-8 waveguide substrate. The tip of the incidence fiber was visually aligned close to the center location of SU-8 waveguide array. The assembled probe was then placed in an aluminum holder to facilitate the probe testing (Figs. 17 and 18). The overall dimension of the sensor probe is $5\times5\times12mm^3$, which is small enough and suitable for ex-vivo esophagus measurements. [22].

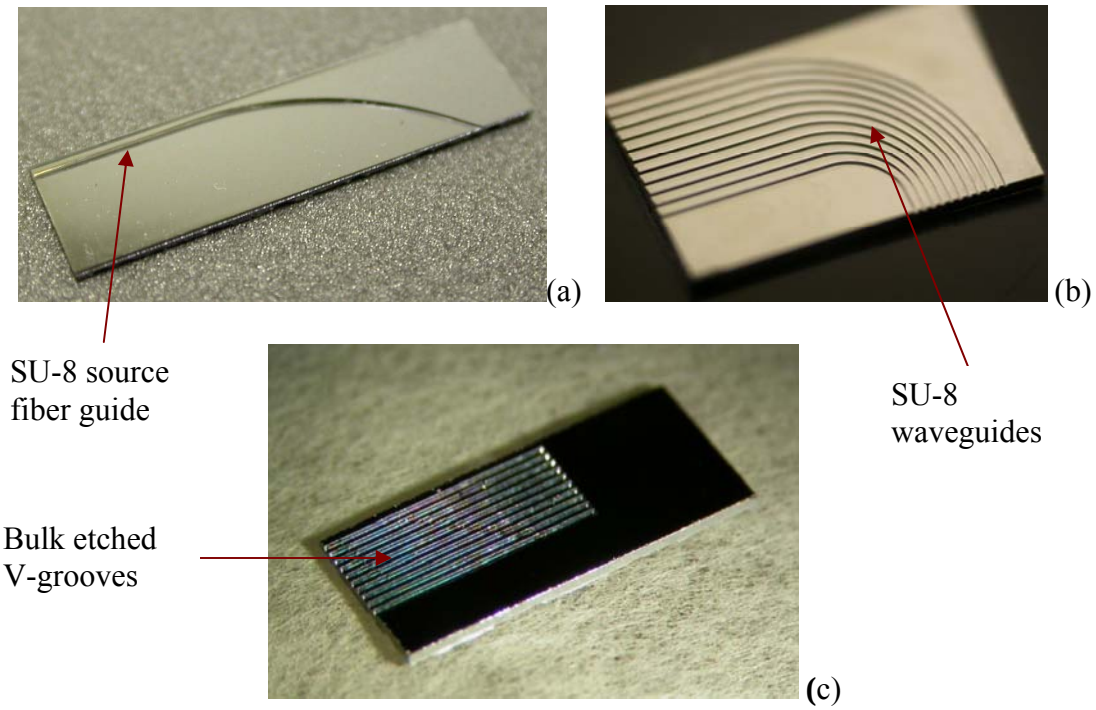

Fig. 16. Micromachined silicon positioning substrates for the OIDRS probe: (a) Source fiber guide; (b) Collection waveguide substrates; and (c) Interconnection fiber guide

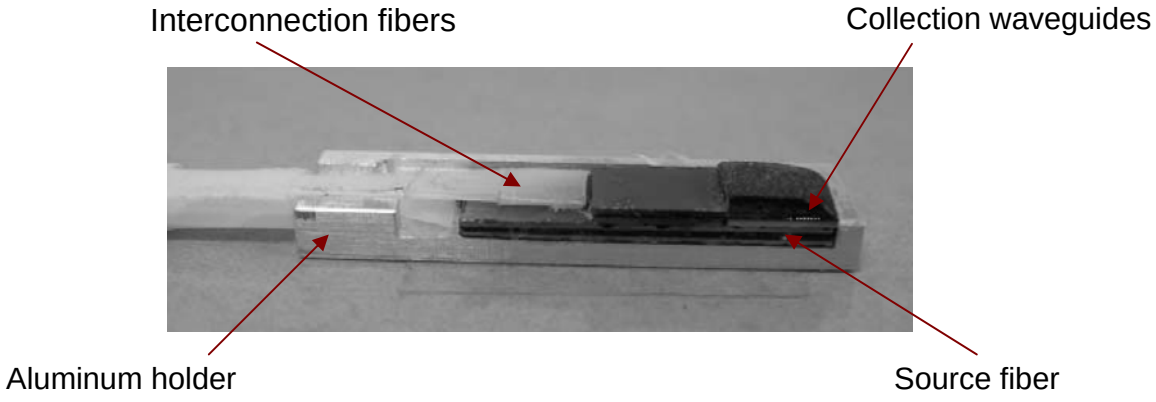

Fig. 17. An assembled probe head

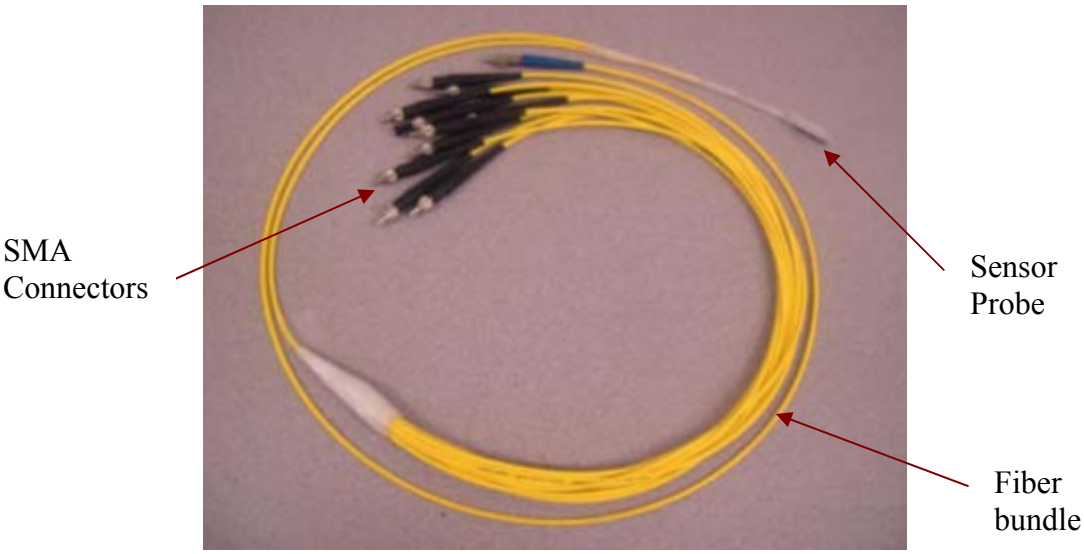

Fig. 18. Complete probe

Calibration of Sensor Probe

Before the actual OIDRS measurement was conducted, the experimental setup was calibrated and validated using a liquid reference solution or phantom consisting of polystyrene micro-spheres as scattering elements and trypan blue as absorber [17]. The absorption coefficient spectra of trypan blue were measured by collimated transmission before mixing it with the polystyrene micro-spheres. The reduced scattering coefficient of the microspheres was calculated using Mie theory [23]. The "expected values" of the absorption and reduced scattering coefficients of the liquid reference solution can be varied by controlling the concentration of absorbing and scattering chemicals.

To conduct the calibration, the senor probe was placed on the surface of the reference solution. The probe was rotated to four different angles with respect to an arbitrary reference point, and the diffuse reflectance was recorded each time. The absorption and reduced scattering spectra were extracted for each diffuse reflectance

measurement and averaged to obtain the "estimated values". The system was calibrated by measuring several optical reference phantoms. The reading from each collection fiber channel is compensated by a factor that matches the "estimated" diffuse reflectance to their expected values (Fig, 19). After the calibration, the probe is ready for measurements on actual esophagus samples. [22]

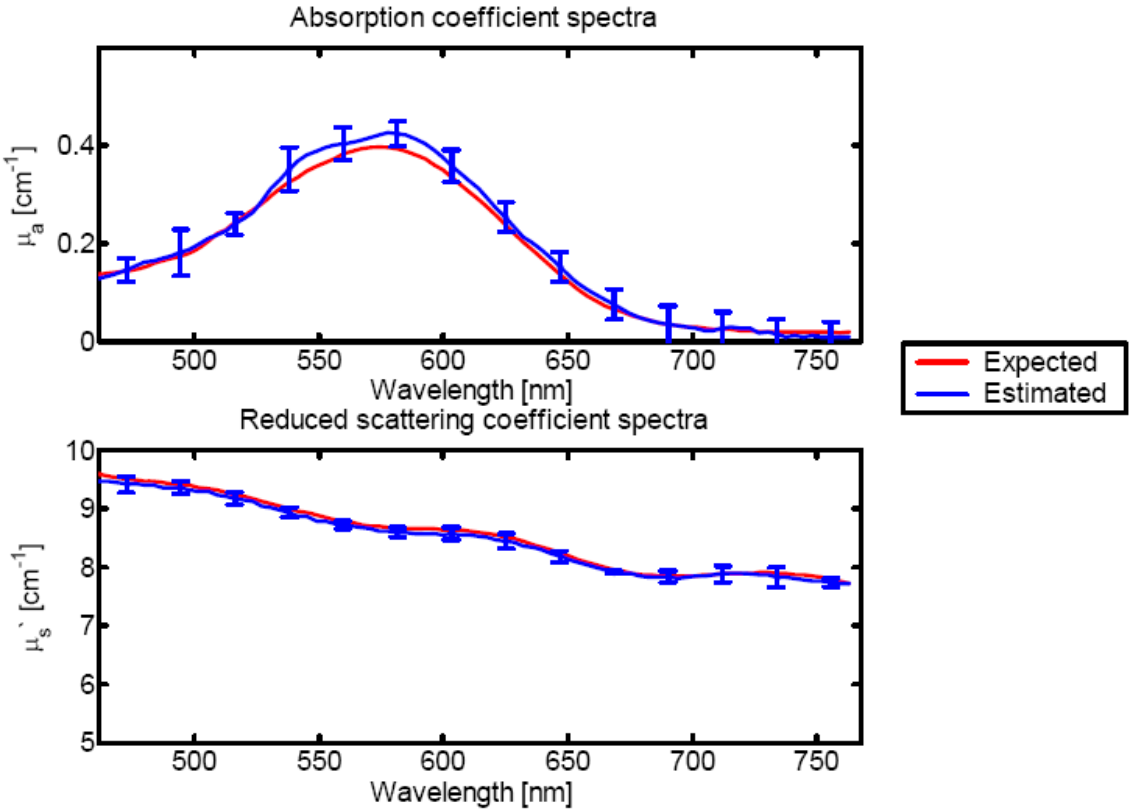

Fig. 19. Expected and estimated absorption and reduced scattering spectra of a liquid reference solution

Ex-Vivo Testing

After the calibration, the OIDRS system and were probe (Fig. 20) were ready for conducting ex-vivo measurement of fresh esophageal biopsy samples at the Barrett's's Esophagus Endoscopy Unit of Mayo Clinic (Rochester, MN). Each sample is approximately ~7 to 8 mm in diameter and 0.4 cm in height (Fig. 21). A total of 20 samples were measured. The samples were collected by endoscopic mucosal resection of the esophageal lining. This minimally invasive technique allows safe and efficacious removal of esophageal tissue. The measurement was performed within 5 minutes after the biopsy was performed. During each measurement the probe is placed at the center of the sample, a total of 4 measurements were conducted on each sample with a 90 degree rotation between each measurement. The samples were later histopathologically analyzed following the standard procedure at the Mayo Clinic. The 20 esophageal samples were found to consist of 8 benign, 6 low dysplastic, 4 highly dysplastic and 2 cancerous lesions.

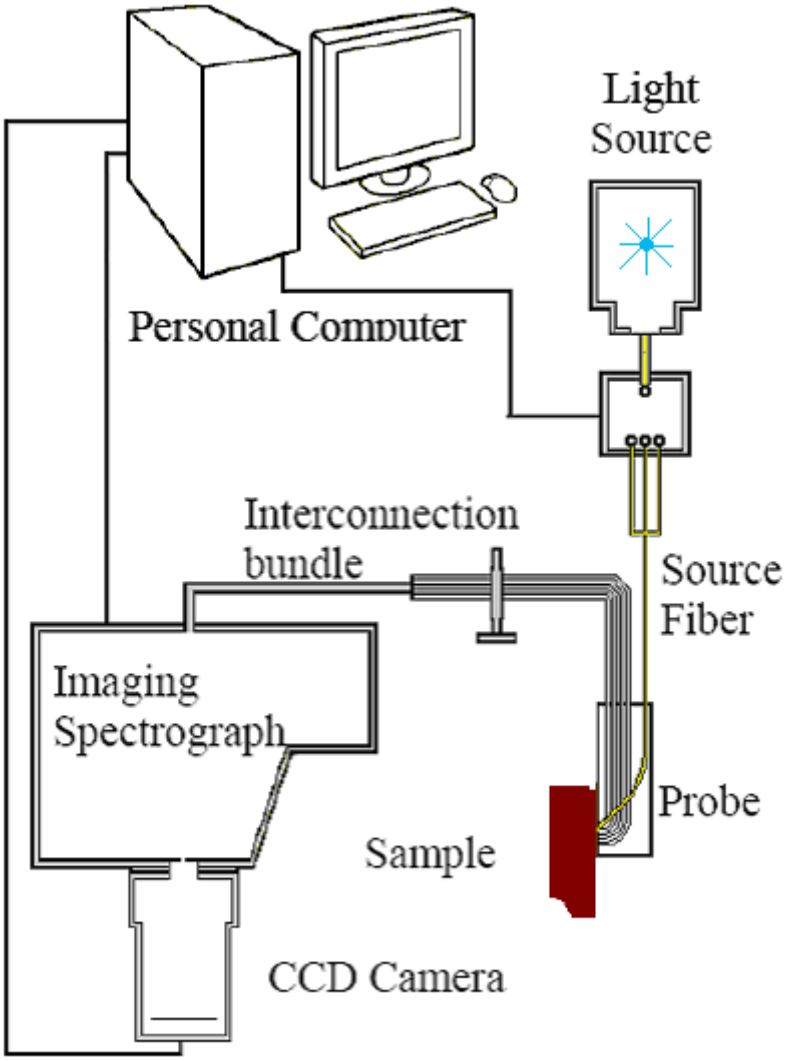

Fig. 20. OIDRS setup for testing esophageal cancer samples

Fig. 21. Esophageal biopsy sample

Figure 22 shows the average OIDRS data, after normalization by the light source, from the middle eight collection channels, for each type of lesion. Due to the small size of the esophageal samples and the unknown diagnostic information the diffuse reflectance was not calibrated with the data from the surrounding normal tissue. The collected data was used to design two classifiers to match the histopathological diagnosis. The first one separates benign and low dysplastic from high dysplastic and cancerous lesions. The second classifier distinguishes benign lesions from low dysplastic ones. Due to the small sample size and the low number of cancerous samples, cancerous cases were combined with the high dysplastic ones.

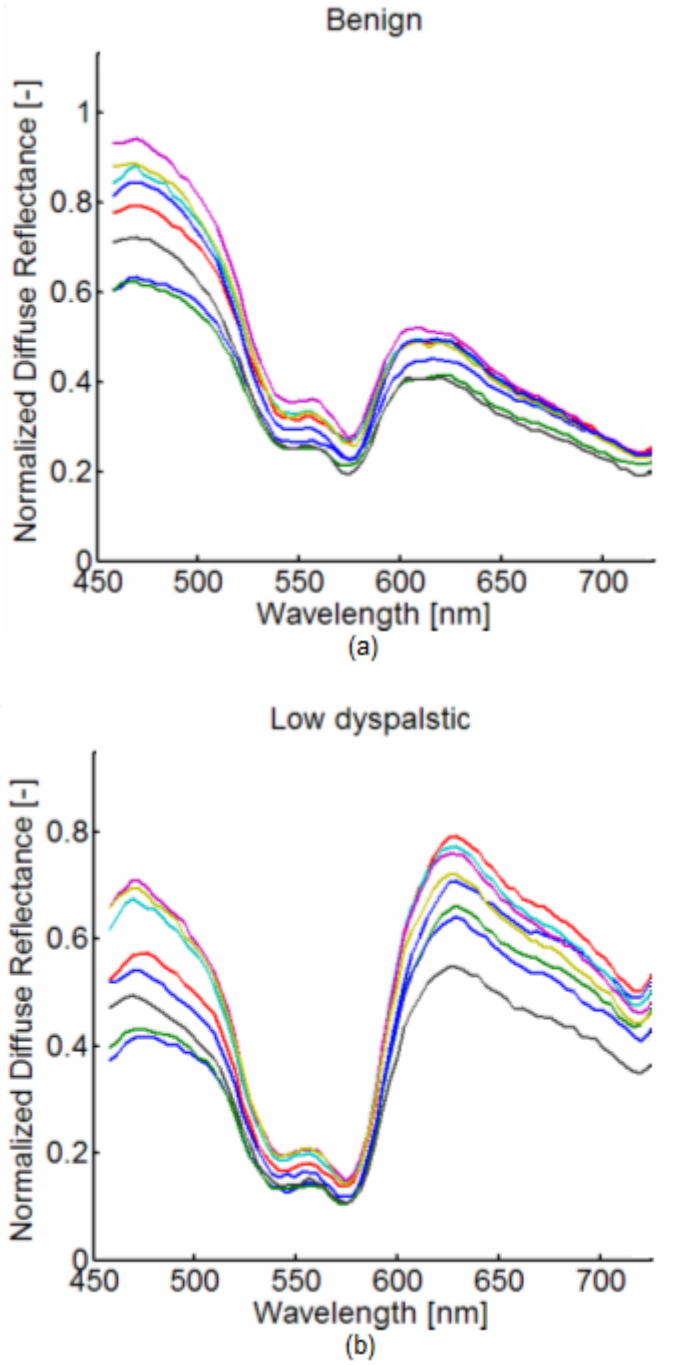

Fig. 22. Average spatio-spectra OIDRS image from the fresh esophageal biopsy samples. (a) benign; (b) low dysplastic; (c) high dysplastic and (d) cancerous

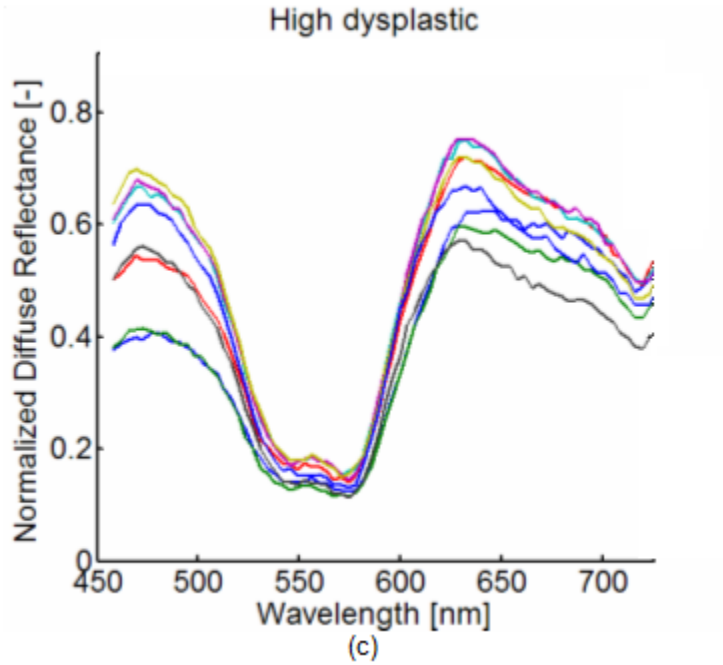

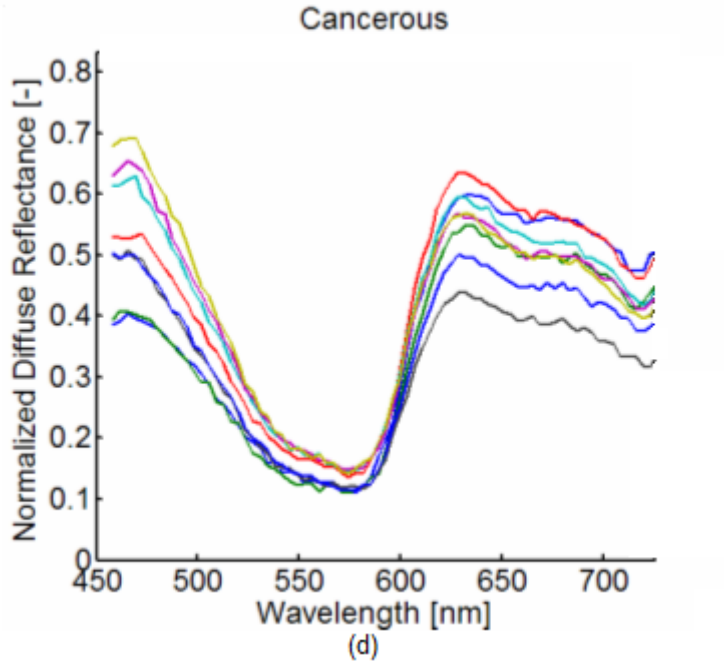

Fig. 22. Continued

Data Classification

Because of the limited number of samples, a bootstrap-based Bayes classifier [24] was used for each group based on the effective features for that group. The leave-one-out method was used for testing. Using this method, one sample from a lesion group was left out, and the bootstrap samples were generated separately for each class using the remaining samples.

The classifier was tested on the left-out sample, and the classification based on this classifier was recorded. This procedure was repeated by inserting the left out sample, taking out a different sample, and then regenerating a new set of bootstrap samples. The procedure is repeated until each of the lesion samples had been individually removed and the classifier tested with all of the left-out samples. Both designed classifiers generated a classification rate of 100% (Figs. 23 and 24).

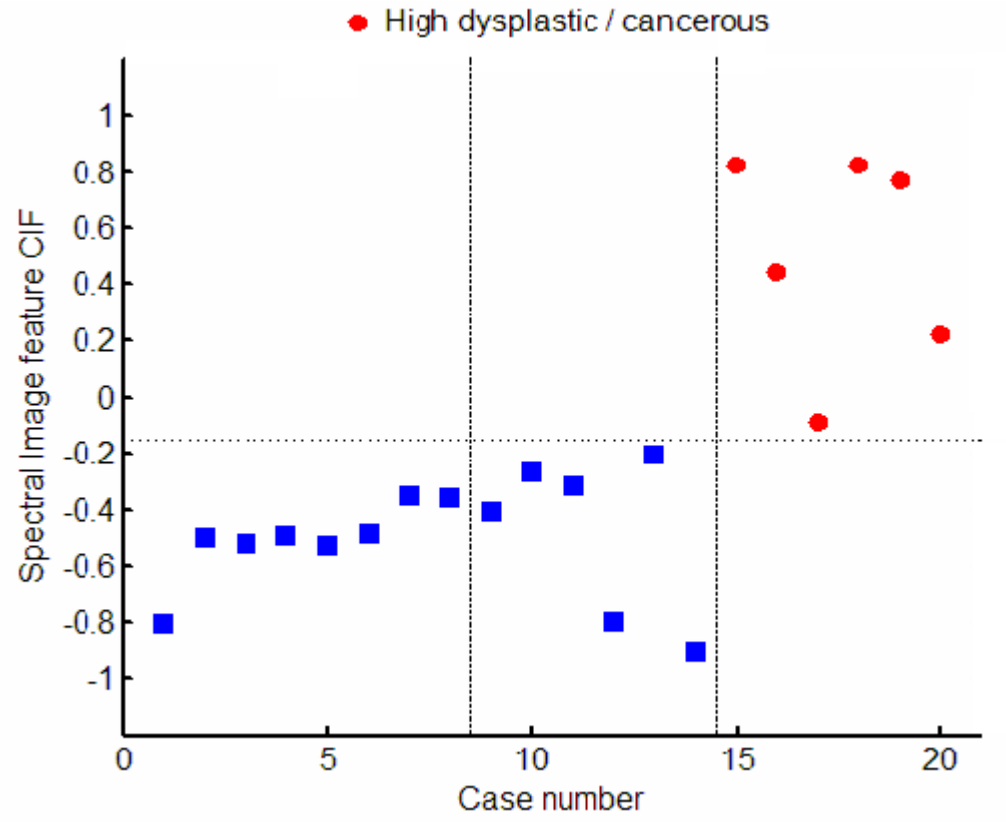

Fig. 23. Classification results of esophageal biopsy samples: benign/low dysplastic vs. high dysplastic/cancerous

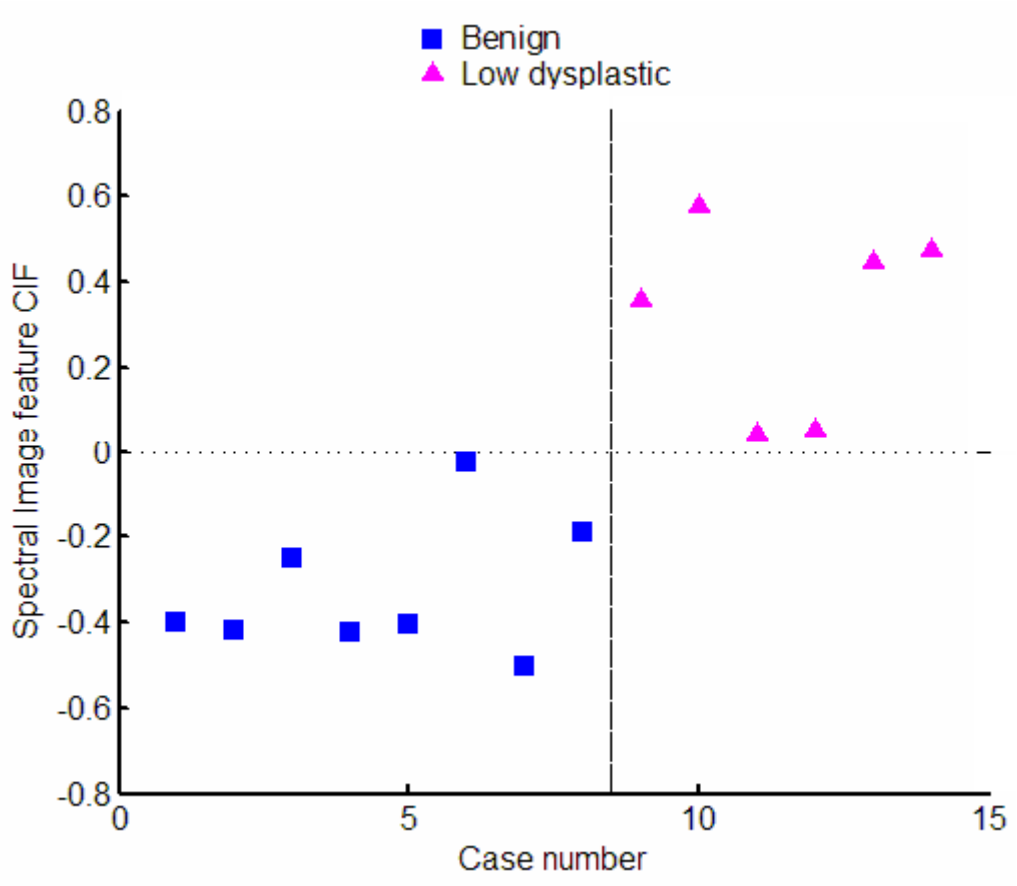

Fig. 24. Classification results of esophageal biopsy samples: benign vs. low dysplastic

CHAPTER V

CONCLUSIONS

A micro-machined sensor probe has been designed and developed using micromachining technology. This probes interfaces with the previously designed OIDRS system and is capable of being used to detect esophageal cancer. The device miniaturization and fabrication precision provided by micromachining ensure reliable and repeatable high performance of the probe.

The main feature of this probe that separates it from the skin cancer probe is its side-viewing capability and reduced size. This probe was tested in an ex-vivo setting with esophageal lesions. Two classifiers were designed during this study. The first one was used to distinguish benign and low dysplastic from high dysplastic and cancerous lesions. The second was used to distinguish between benign lesions and low dysplastic ones. Preliminary results on a data set of 20 lesions indicate a classification rate of 100% with both classifiers. The information provided by this system can potentially be used to assist in the diagnosis and classification of, esophageal and other organs pathologies.

REFERENCES

1. American Cancer Society website, What Are the Key Statistics About Cancer of the Esophagus?, http://www.cancer.org, (2008), 02/01/2009.
2. Commons Wikimedia, Barrett's Esophagus.jpg http://commons.wikimedia.org/wiki/File:Barretts_esophagus.jpg, 02/10/2009.
3. N. Ramanujam, M.F. Mitchell, A. Mahadevan, S. Warren, S. Thomsen, E. Silva, R. Richards-Kortum, R. *Proc. Natl. Acad. Sci. USA*, 1994, **91** (21), 10193–10197.
4. Nath, K. Rivoire, K.; S. Chang, L. West. S. B. Cantor, K, Basen-Engquist, K Adler-Storthz, D. D. Cox, E. N. Atkinson, G. Staerkel, C. MacAulay, R. Richards-Kortum, M. Follen, *Int. J. Gynecol. Cancer*, 2004, **14** (6), 1097–1107.
5. S. Tomatis, C. Bartoli, A. Bono, N. Cascinelli, C. Clemente, and R. Marchesini, *Journal of Photochemistry & Photobiology. B –Biology,* 1998, **42**, 32-39.
6. D Arifler, C. MacAulay, M. Follen, R Richards-Kortum, *J. Biomed. Opt,* 2006, **11** (6), 064027.
7. Y.N. Mirabal, S.K.; Chang, E.N Atkinson, A Malpica, M Follen, R Richards-Kortum, *J. Biomed. Opt.,* 2002, **7** (4), 587–594.
8. A. G. Bohorfoush, *Endoscopy,* 1996, **28**, 372-380.
9. J. R. Mourant, I. J. Bigio, J. Boyer, T. M. Johnson, J. Lacey, A. G. Bohorfoush, and M. Mellow, *J. Biomed. Opt*., 1996, **1**, 192-199.
10. T. L. Troy, D. L. Page, and E. M. Sevick-Muraca, *J. Biomed. Opt*., 1996 **1**, 342-255.

11. I.J. Bigio, S.G. Bown, G. Briggs, C. Kelley, S. Lakhani, D Pickard, P.M Ripley, I.G Rose, C. Saunders, *J. Biomed. Opt.,* 2000, **5** (2), pp. 221–228.

12. S.-P. Lin, L.-H. Wang, S. L. Jacques, and F. K. Tittel, " *Applied Optics,* 1997, **36** (1), 136–143.

13. V. Backman, M. B. Wallace, L. T. Perelman, J. T. Arendt, R. Gurjar, M. G. Muller, Q. Zhang, G. Zonios, E. Kline, T. McGillican, S. Shapshay, T. Valdez, K. Badizadegan, J. M. Crawford, M. Fitzmaurice, S. Kabani, H. S. Levin, M. Seiler, R. R. Dasari, I. Itzkan, J. Van Dam , M.S. Feld., *Nature,* 2000, **406**, 35-36.

14. H. B. Stone, J. M. Brown, T. L. Phillips, and R. M. Sutherland, *Radiation Research,* 1993, **136**, 422-434.

15. H. B. Jiang, J. Pierce, J. Kao, and E. Sevick-Muraca, *Appl. Opt.,* 1997, **36**, 3310-3318.

16. S. -P. Lin, L. Wang, S. L. Jacques, and F. K. Tittel, *Appl. Opt.*, 1997, **36**, 136-143.

17. G. Marquez and L.-H. Wang, *Optics Express,* 1997, **1**, 454-460.

18. S. -P. Lin, L. Wang, S. L. Jacques, and F. K. Tittel, *Appl. Opt*., 1997, **36**, 136-143.

19. H. C. van de Hulst, *Light Scattering by Small Particles*, Dover Publications, Inc., New York, 1981.

20. L. V. Wang and H.-i Wu, *Biomedical Optics: Principles and Imaging*, Wiley-Interscience, New York, 1st edn., 2007.

21. A. Garcia-Uribe, K. C. Balareddy, J. Zou and L. V. Wang, *IEEE Sensors Journal*, 2008, **8** (10), 1698-1703.

22. A. Garcia-Uribe, K. C. Balareddy, J. Zou, A. Wojcik, L. V. Wang and K. K. Wang, *Sensors and Actuators A: Physical,* 2009, **150** (1), 144-150.

23. T. J. Farrell and M. S. Patterson, *Med. Phys*., 1992, **19**, 879–888.

24. B. Efron and R, Tibshirani, *Statistical Science*, 1986, **1** (1), 54-75.

VITA

Karthik Reddy Chinna Balareddy received his Bachelor of Science degree in electrical engineering from Texas A&M University in May 2006. He entered the Electrical Engineering program at Texas A&M University in August 2006 and received his Master of Science degree in May 2009. His research interests include MEMS, optical probes and application of microfabrication and micromachining in the medical field. He plans to pursue a Ph.D. in electrical engineering and continue research in these fields.

Mr. Chinna Balareddy may be reached at the Department of Electrical and Computer Engineering, 214 Zachry Engineering Center, Texas A&M University, College Station, TX–77843. His email is karthik06@gmail.com.